Journal of Nuclear Research and Applications

Research Paper

Vol. 2, No. 3, 2022, P 12-18

Cited in: https://jonra.nstri.ir
Received: 2 May 2022, Accepted: 15 May 2022

Shape Changes in Odd-Even Osmium Isotopes

M. Moonesi*, S. Mohammadi, M. Shahriari

Department of Physics, Payame Noor University, P. O. BOX 19395-3697 Tehran, Iran

ABSTRACT

This paper has calculated the energy levels of $^{185\text{-}187\text{-}189}$Os isotopes using the projected shell model (PSM). Yrast Spectrum, nucleus rotation frequency and the ratio of reduced electromagnetic transition probabilities, B(E2)/B(M1) plots versus spin for understanding the structure of multi-quasiparticle band up to the spins $47/2^+$, $33/2^+$ and $31/2^+$ for these isotopes, are plotted, respectively. It was found that in the spin ranges $35/2^+$-$39/2^+$, $31/2^+$-$33/2^+$, and $27/2^+$-$29/2^+$, due to 3-quasiparticle band-crossing, simultaneously by increasing rotational inertia of the nucleus, nucleus rotation frequency decreases greatly and as an important result, B(E2)/B(M1) ratio, the electrical properties of the nucleus in these spins increase. Indeed, in these isotopes, observed that by increasing neutron number, the deformation parameter, ε_2 decreases as well, and by increasing spin in especial spins, due to nucleon alignment phenomenon, the nucleus rotational behavior decreases inverse the vibration mode.

***Keywords*:** Yrast Spectrum, Alignment Phenomenon, Electromagnetic Transition Probability, Projected Shell Model.
***PACS Nos*:** 21.60.-n

I. Introductions

The electromagnetic spectrum of the gamma rays resulting in the excited nucleus in high spin always for studying nuclear structure was important. Especially, for neutron-rich heavy deformed nuclei in the rare-earth region with 180 < A < 200, in the past few years, it was caused that using nuclear spectroscopic techniques change has changed and these nuclei show new band structures [1-3]. Very few theoretical and experimental studies have been reported with the aim of understanding the osmium isotopes. Some of the important research on these isotopes are reported, which among them the experimental works was carried out by S. Mohammadi et al. [4-7], high-spin states in the neutron-rich nuclei of $^{184\text{-}186\text{-}188\text{-}190}$Os [5-6] and $^{185\text{-}187\text{-}191}$Os [7] have been populated using the ^{85}Se+^{192}Os deep-inelastic reaction.

The theoretical work was carried out by the projected shell model for the first time by Nilsson in 1955 [8] for considering to consider the deformed shape of the nucleus was presented. Forty-five years later, this model was formulated as a shell model projected on the nuclear symmetry axis known as the PSM by Hara and Sun [9]. Finally, in 1997, the FORTRAN code of the PSM for PCs was written and published [10] and has

*Corresponding Author name: M. Moonesi
E-mail address: maryammoonesi63@gmail.com

been quietly successful and is still used today.

By the PSM code, many articles have been published, including for Osmium and Erbium, back-bending and nucleon-rich phenomenon due to the reduced electromagnetic transition probabilities, B(M1)/B(E2), by Shahriari et al [11] and Moonesi et al [12], calculated and compared with the experimental values.

In the present work, the main purpose is a systematic study of the effect of increasing neutrons number on the deformation parameter, ε_2, and nucleus rotation mode in slightly high spin states of $^{185\text{-}187\text{-}189}$Os isotopes by use of the projected shell model.

In section 2, the projected shell model (PSM), section 3 results and discussion, and in section 4, the conclusions are summarized.

II. Projected Shell Model

The PSM is a truncated spherical shell model projected on axial symmetry of deformed nuclei and most commonly is used to study medium and heavy-rare-earth mass nuclei. The PSM's most important is forming a quasi-particle structure by combining the single-particle deformed states from the Nilsson model with the BCS calculations based on the vacuum quasi-particle, |0> [13]. The configuration space of the PSM model generally consists of three major shells for protons and neutrons. In this model, Computations are done with three major shells N= 3, 4, 5 (N=4, 5, 6) with active shell N=5 (N=6) for protons (neutrons). Nilsson parameters ε_2 (Quadrupole deformation) and ε_4 (Hexadecupole deformation) are chosen from Ref. [14] and are listed in Table 1. By projecting a set of multi-quasiparticle states $|\Phi_k>$ that includes single and three-particle states for the odd-even nuclei in the form of the relation 1 on a suitable angular momentum such as I, quasi-particle states of the deformed shell model are constructed.

$$\{|\Phi_k>\} = \left\{a_\upsilon^\dagger|\,0>.\,a_\upsilon^\dagger a_{\pi_1}^\dagger a_{\pi_2}^\dagger|0>\right\} \quad (1)$$

Where |0> the vacuum state and $a^\dagger$ are the quasi-particle (qp) creation operators and the index $\upsilon(\pi)$ stands for neutrons (protons). Then by defining the angular momentum image operator $\hat{P}^I_{MK}$ as [3]:

$$\hat{P}^I_{MK} = \frac{2I+1}{8\pi^2}\int d\Omega\, D^I_{MK}(\Omega)\hat{R}(\Omega) \quad (2)$$

So that $\hat{R}(\Omega)$ is the rotational operator, Ω the Euler angle, and $D^I_{MK}(\Omega)$ the function –D, which forms a complete set of functions in the parametric space Ω by affecting the nucleon-like pairs. $|\Phi_k>$, wave function form of the PSM is obtained.

$$|\Psi_{IM}> = \sum_K F^I_K \hat{P}^I_{MK}|\Phi_k> \quad (3)$$

Coefficients F^I_K by solving the Schrodinger equation $\hat{H}\,|\Psi_{IM}> = E\,|\Psi_{IM}>$ and simultaneous Hamiltonian diagonalization are determined at the bases $\{\hat{P}^I_{MK}|\Phi_k>\}$ As a result, the eigenvalue equation of the PSM is obtained as:

$$\sum_{k'}\left(H^I_{kk'} - E\,N^I_{kk'}\right)F^I_{k'} = 0 \quad (4)$$

So that the elements of the Hamiltonian and normal matrixes are defined as 5 relations,

(5)

$$N^I_{kk'} = \langle\Phi_k|\hat{P}^I_{kk'}|\Phi_{k'}\rangle,$$
$$H^I_{kk'} = \langle\Phi_k|\hat{H}\hat{P}^I_{kk'}|\Phi_{k'}\rangle$$

Finally, the amount of energy required for the Hamiltonian model of Nilsson is obtained as a function of spin I, which is used for a spin (band diagram energy) as:

$$E(I) = \frac{\langle\Phi_k|\hat{H}\hat{P}^I_{kk'}|\Phi_{k'}\rangle}{\langle\Phi_k|\hat{P}^I_{kk'}|\Phi_{k'}\rangle} = \frac{H^I_{kk'}}{N^I_{kk'}} \quad (6)$$

The Hamiltonian used in these calculations by equation (7), Eigen energies of quasi-particles were obtained. More details of the PSM theory calculations are defined in Ref. [9]:

$$H = H_0 - \frac{1}{2}\chi\sum_\mu \hat{Q}^+_\mu\hat{Q}_\mu - G_M\hat{P}^+\hat{P} - G_Q\sum_\mu \hat{P}^+_\mu\hat{P}_\mu \quad (7)$$

H_0 is a harmonic oscillator single-particle Hamiltonian containing a proper spin-orbit force. The second, third, and fourth expressions, which form the non-spherical Hamiltonian, represent quadrupole-quadrupole, monopole, and quadruple-pairing interactions, respectively. The Coefficients of χ, G_M, and G_Q are called strength of interactions. The value of strength, χ can be calculated self-consistently using the deformation parameter ε_2. The monopole paring strengths, G_M can be expressed by equation 8:

$$G_M = \left[21.20 \pm 13.90 \frac{N-Z}{A}\right] A^{-1} \quad (8)$$

where the (-) sign is for neutrons and the (+) sign for protons. The G_Q quadrupole coupling power is assumed to be proportional to G_M and is considered to be a constant at 0.16 [15].

Table 1. Quadrupole and Hexadecupole deformation parameters are used in the present calculation.

Os	185	187	189
ε_2	0.2	0.19	0.18
ε_4	0.07	0.08	0.08

III. Results and Discussions

III.I Yrast spectra structure

In this section, by using PSM code which was written based on the Nilsson model in deformed single particles states [3], Yrast spectra which consist of a collection of the bands in the lowest energies after diagonalization of the Hamiltonian, Eq. (7) , in the projected basis, Eq. (1), for $^{185\text{-}187\text{-}189}$Os isotopes in the spin ranges $9/2^+$-$47/2^+$, $9/2^+$-$33/2^+$ and $9/2^+$-$31/2^+$ for the theoretical values are shown in Figs. 1 a., b. and c., respectively. Also, the experimental values for the Yrast line with theoretical values are plotted and compared in Fig.2. Appropriate experimental data for ^{189}Os was not found. The details are as follows:

a. ^{185}OS: The Yrast line up to spin $37/2^+$ is made up of two single neutron bands $1\upsilon\, i_{13/2}[-7/2]$, K=-7/2, $1\upsilon\, i_{13/2}[9/2]$ K=9/2. At spin I=37/2, these two 1-qp neutrons bands cross 3-qp bands having configuration $1\upsilon i_{13/2}[-9/2] + 2\pi h_{11/2}[9/2, 5/2]$, K=5/2 $\upsilon i_{13/2}[9/2] + 2\pi h_{11/2}[-3/2, 1/2]$, K=7/2 where their energies decrease and approach to the Yrast line. Therefore, the spin range of $9/2^+$ to $37/2^+$ of the Yrast line contains single-particle bands and in the spin range of $I \geq 37/2$ contains 3-qp (2-qp protons plus 1qp-neutron) bands.

b. ^{187}OS: The Yrast line up to spin $29/2^+$ is made up of two single neutron bands $1\upsilon\, i_{13/2}[-11/2]$, K=-11/2, $1\upsilon\, i_{13/2}[9/2]$ k=9/2. At around spin I=29/2, $1\upsilon\, i_{13/2}[-11/2]$, K=-11/2 1qp neutron band cross 3-qp bands having configuration $1\upsilon i_{13/2}[9/2] + 2\pi h_{11/2}[-9/2,-5/2]$, K=-5/2, $1\upsilon i_{13/2}[-11/2] + 2\pi h_{11/2}[-9/2,9/2]$, K=-11/2 where their energies decrease and approach to the Yrast line. So in the spin range of $11/2^+$ to $29/2^+$ the Yrast line contains single-particle bands and in the spin range of $I \geq 29/2$ includes 3-qp (2-qp protons plus 1qp-neutron) bands.

c. ^{189}OS: The Yrast line up to spin $19/2^+$ is made up of two single neutron bands $1\upsilon\, i_{13/2}[-11/2]$, K=-11/2, $1\upsilon\, i_{13/2}[9/2]$ K=9/2. At spin I=19/2, these two 1-qp neutrons bands cross each other and change their positions. At spin 23/2, $1\upsilon\, i_{13/2}[-11/2]$, K=-11/2 1qp neutron band cross 3-qp band $1\upsilon i_{13/2}[9/2] + 2\pi h_{11/2}[11/2, -3/2]$, K=17/2 and their energy decreases and approaches to the Yrast line. So in the spin range of $9/2^+$ to $23/2^+$ the Yrast line contains single-particle bands and in the spin range of $I \geq 23/2$ includes 3-qp (2-qp protons plus 1qp-neutron) bands.

III. II Alignment phenomenon

As was shown in Figs 1 a., b. and c., the Yrast line has a slight slope change concerning spin. Since the rotation frequency in terms of spin represents a major quantity to describe the band diagram of nuclei, Fig. 3 shows rotation frequency versus spin for $^{185\text{-}187\text{-}189}$Os isotopes. The nucleus rotation frequency, ω versus spin, that shows nucleon alignment the nucleus is known as the “alignment phenomenon” and is defined by the following relation:

$$\omega = \frac{E(I) - E(I-\Delta I)}{\Delta I} (h^{-1}\,MeV) \quad (9)$$

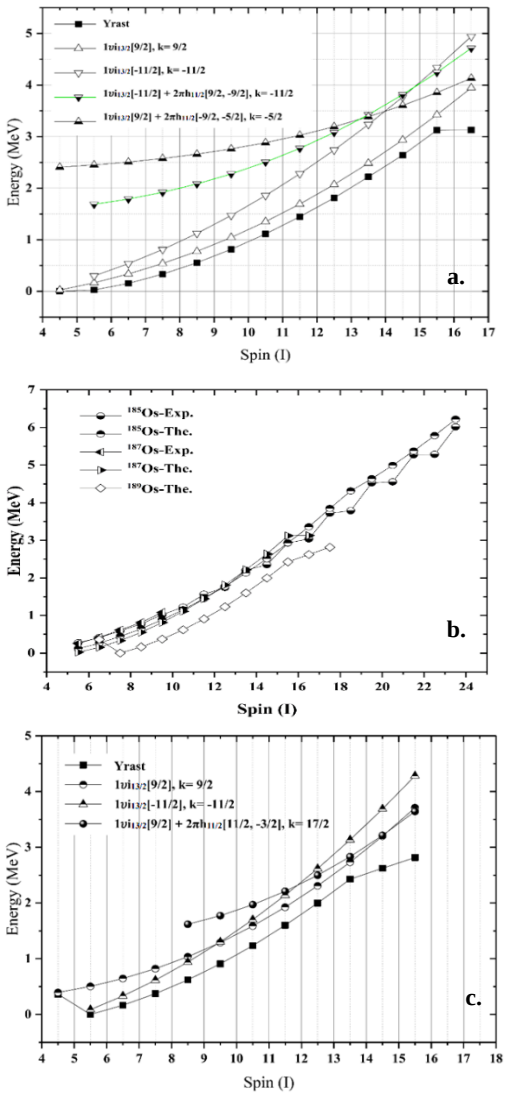

Fig. 1. The band diagram and the Yrast line for **a.** ^{185}Os and **b.**^{187}Os and **c.** ^{189}Os.

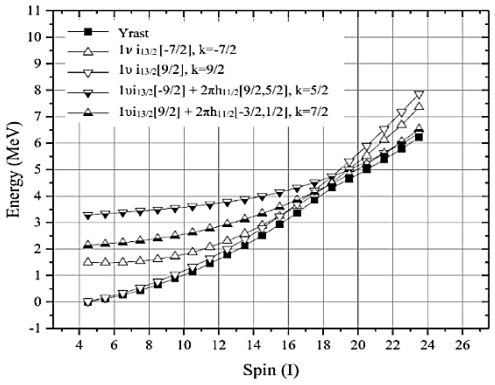

Fig. 2. Comparison of the theoretical with experimental values of the Yrast line for ^{185}Os[16] and $^{187\text{-}189}$Os [17].

Where for double-odd isotopes ΔI=1, As is shown in Fig. 3, there are some irregularities concerning spin. The details are as follows:

a. **^{185}Os**: Rotation frequency starts at spin $11/2^+$ and reaches a maximum at spin $35/2^+$, and after that, it starts to reduce. By comparing this alignment diagram with the band diagram in Fig. 1 a, this phenomenon of reduction rotation frequency versus spin increase can be related to breaking down a pair of protons at spin $39/2^+$ and forming two quasi-particles, as mentioned before.

b. **^{187}Os**: Rotation alignment starts at spin $13/2^+$ and reaches a maximum at spin $31/2^+$ and suddenly drops to a minimum at spin $33/2^+$. By comparing with Fig.1 b, again, this phenomenon can be related to the breaking down of a pair of protons, thus increasing the moment of inertia and decreasing rotation frequency.

c. **^{189}Os:** Rotation alignment starts at spin $13/2^+$ and reaches a maximum at spin $27/2^+$ and suddenly drops to a minimum at spin $29/2^+$. By comparing with Fig. 2, this phenomenon can be related to the breaking down of a pair of protons and forming two quasi -particles, thus increasing the moment of inertia and decreasing rotation frequency in this isotope.

As it can be seen in Fig. 3, it has been specified that the rotation of quasi-particle bands around the nucleus exactly depends on the quadrupole deformation ε_2, and by increasing the number of core nucleons (mass number), according to Table 1, deformation decreases.

For the $^{185\text{-}187\text{-}189}$Os, isotopes nucleons pair with a downward process in the states with spins $39/2^+$, $33/2^+$, and $29/2^+$. Indeed, one pair of protons 2-qp in h11/2 intruder level was broken and were coupled with neutron 1-qp nucleons bands aligned and rotated with core spin. This event caused to reduced nucleus rotational frequency, ω, and core rotational inertia increases. Indeed, slightly, by shifting the rotational behavior to vibrational one, from the Nilsson diagram, this phenomenon can also be seen as the motion of paired protons from 9/2 [514] orbital towards 1/2[411] orbital with a decrease of deformation parameter.

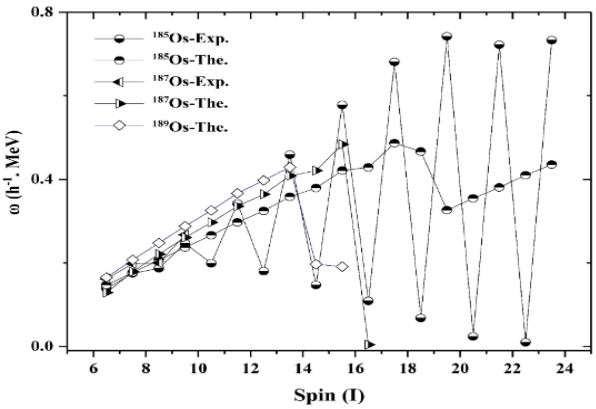

Fig. 3. Comparison of theoretical with experimental values of the alignments phenomenon for the Yrast line for ^{185}Os [16] and $^{187\text{-}189}$Os [17].

III.III. B (E2) / B (M1) ratio

Another important quantity related to the band diagram and alignment phenomenon in nuclei is the reduced electric quadrupole and magnetic dipole transition probabilities, B (E2) and B (M1), that can be calculated using PSM wave functions [18], Eq. (1), from the initial state (I_i = I) to the final state (I_f = I-2) and (I_f =I-1), respectively, is given by [9]:

$$B(E2, I \to I-2) = \frac{e^2}{(2I+1)} |\langle \Psi^{I-2} || \hat{Q}_2 || \Psi^{I} \rangle|^2 \quad (10)$$

$$B(M1, I \to I-1) = \frac{\mu_N^2}{(2I+1)} |\langle \Psi^{I-1} || \hat{M}_1 || \Psi^{I} \rangle|^2 \quad (11)$$

Where $|\Psi^I>$ denotes the wave functions and $|\langle \Psi^{I_f} || \hat{O}_L || \Psi^{I_i} \rangle|^2$ is the reduced matrix element of an operator $\hat{O}$ ($\hat{O}$ is either $\hat{Q}$ or $\hat{M}$) which expressed by

$$< \Psi^{I_f} || \hat{O}_L || \Psi^{I_i} > = \sum_{k_i . k_f} f_{K_i}^{I_i} \, f_{K_f}^{I_f} \sum_{M_i . M_f . M} (-)^{I_f - M_f} \begin{pmatrix} I_f & L & I_i \\ -M_f & M & M_i \end{pmatrix} \times \left\langle \phi_{kf} \middle| \hat{P}^{I_f}_{K_{kf} M_f} \hat{O}_{LM} \hat{P}^{I_i}_{K_{ki} M_i} \middle| \phi_{ki} \right\rangle \quad (12)$$

$\hat{Q}_2$ that point to the electric quadrupole operator was defined by relations

$$\hat{Q}_{2\upsilon} = e_\upsilon^{eff} \sqrt{\frac{5}{16\pi}} \, Q_\upsilon^2 \quad \text{(neutrons)},$$

$$\hat{Q}_{2\pi} = e_\pi^{eff} \sqrt{\frac{5}{16\pi}} \, Q_\pi^2 \quad \text{(protons)} \quad (13)$$

and the effective charge is 0.5e for neutron and 1.5e for proton, respectively. $\hat{M}_1$ point to the magnetic dipole operator was defined by $\hat{M}_1^\tau = g_l^\tau \hat{j}^\tau + (g_s^\tau - g_l^\tau) \hat{s}^\tau$, that τ likes to be either υ for neutron or π for proton, g_l and g_s are the orbital and spin gyromagnetic factors, respectively [19]. In this paper, in the PSM calculation, the standard values of g_l, and g s for free protons and neutrons used are g_l^π= 1, g_l^υ=0 and g_s^υ = -3.82 and g_s^π=5.58.

To account for core-polarization and meson-exchange currents, g_s^π and g_s^υ values are damped by a correction factor of 0.75 [20, 21]. Finally, by considering the mean lifetime, τ in each transition, the reduced transition probabilities B (E2) and B (M1) are obtained as [22]:

$$B(E2) = \frac{816}{E_\gamma^5 \, \tau_p} e^2 \text{ fm}^4 \text{ MeV}^5 \text{ ps} \quad (14)$$

$$B(M1) = \frac{56 \cdot 8}{E_\gamma^3 \, \tau_p} \mu_N{}^2 \text{ MeV}^3 \text{ fs} \quad (15)$$

Where their ratio is:

$$\frac{B(E2)}{B(M1)} = 1 \cdot 44 \, \frac{1}{E_\gamma^2} \frac{e^2 b^2}{\mu_N^2} \text{MeV}^2 \quad (16)$$

This electromagnetic ratio for each of $^{185\text{-}187\text{-}189}$Os isotopes for the Yrast line has been calculated and is shown in Fig. 4. Also, the percentages of electrical behavior for each gamma transition are given in Table 2. The detail for each isotope is as follows:

a. ^{185}Os: As it can be seen from Fig. 4, the electromagnetic ratio B (E2)/B (M1) decreases gradually from spin $\frac{11^+}{2}$ ħ to spin $\frac{37^+}{2}$ ħ. This

means that the nature of gamma transitions in the nucleus is initially mostly electrical, and then with increasing spin and subsequently rotational motion of the nucleus, the contribution of electrical quadrupole property decreases. Because of band crossing of three quasiparticle bands $1\upsilon i_{13/2}$[-9/2] + $2\pi h_{11/2}$[9/2,5/2], K=5/2 , $1\upsilon i_{13/2}$[9/2] + $2\pi h_{11/2}$ [-3/2,1/2], K=7/2 with single-quasiparticle bands $i\upsilon_{13/2}$[-7/2], K=-7/2, 1υ $i_{13/2}$[9/2], K=9/2 which occurs in the spin range $\frac{35^+}{2}$ ħ − $\frac{37^+}{2}$ ħ, rotational motion of nucleus decreases and electrical properties of core increase slightly.

b. ^{187}Os: The electromagnetic ratio B (E2)/B (M1) decreases gradually from spin $13/2^+$ to spin $31/2^+$. This is due to band crossing of three quasiparticle $1\upsilon i_{13/2}$[-11/2] + $2\pi h_{11/2}$[9/2,-9/2], K=-11/2, $1\upsilon i_{13/2}$[9/2]+ $2\pi h_{11/2}$[-9/2,-5/2], K=-5/2 with single quasiparticle bands 1υ $i_{13/2}$[-7/2], K=-7/2, $1\upsilon i_{13/2}$[9/2] K=9/2 which occurs at near spin $\frac{29^+}{2}$ ħ and corresponding to rotational alignment.

c. ^{189}Os: The electromagnetic ratio B (E2)/B (M1) decreases gradually from spin $\frac{13^+}{2}$ ħ to spin $\frac{27^+}{2}$ ħ. Here it is due to band crossing in the spin range $\frac{27^+}{2}$ ħ − $\frac{29^+}{2}$ ħ, of a three-quasiparticle band of two protons and a single neutron, $1\ \upsilon\ i_{13/2}$[9/2] + $2\pi h_{11/2}$[11/2, -3/2], K=17/2 with single-quasiparticle bands 1υ $i_{13/2}$[9/2], K=9/2, 1υ $i_{13/2}$[-11/2] K=-11/2.

As it can be seen from the above discussions, by increasing neutron number, the electromagnetic ratio B (E2)/B (M1) behavior changes for each isotope which is coincident with band crossing and rotation alignments.

Indeed, this increment in B(E2)/B(M1) value, with an increased neutron number, is related to a reduction in electrical quadrupole deformation, ε_2. In addition, a sudden rising in electromagnetic transition occurs, from $29/2^+$ to $39/2^+$ for these isotopes which is coincident with band-crossing and back-bending in rotation alignments.

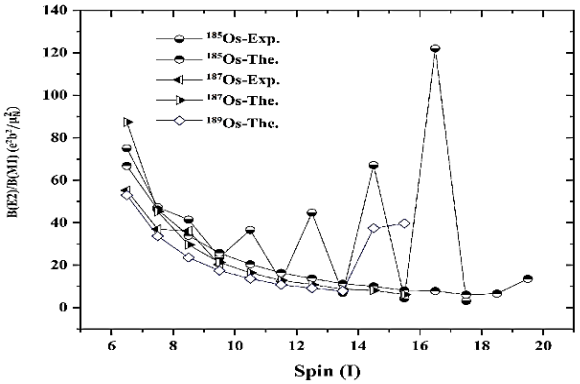

Fig. 4. Ratio of the reduced electromagnetic transition probabilities, B(E2)/B(M1), as a function of spispin function for $^{185\text{-}187\text{-}189}$Os. Experimental data are taken from Refs. [16,17].

Table 2. B(E2)/B(M1) ratio changes with spin and comparison with experimental [16,17] and theoretical value for $^{185\text{-}187\text{-}189}$Os.

Spin			B(E2)/B(M1)					
^{185}Os	^{187}Os	^{189}Os	^{185}Os		^{187}Os		^{189}Os	
			Exp.	The.	Exp.	The.	Exp.	The.
13/2+	13/2+	13/2+	75.01	66.79	55.22	87.36	-	52.97
15/2+	15/2+	15/2+	47.32	46.25	36.96	45.28	-	33.72
17/2+	17/2+	17/2+	41.44	33.92	36.23	29.64	-	23.62
19/2+	19/2+	19/2+	23.75	25.80	20.32	21.30	-	17.47
21/2+	21/2+	21/2+	36.59	20.46	-	16.45	-	13.67
23/2+	23/2+	23/2+	12.39	16.39	-	12.88	-	10.78
25/2+	25/2+	25/2+	44.73	13.78	-	10.92	-	9.17
27/2+	27/2+	27/2+	6.87	11.28	-	8.69	-	7.87
29/2+	29/2+	29/2+	67.06	10.07	-	8.18	-	37.45
31/2+	31/2+	31/2+	4.33	8.18	-	6.19	-	39.68
33/2+	-	-	121.98	7.88	-	-	-	-
35/2+	-	-	3.12	6.11	-	-	-	-
37/2+	-	-	-	6.65	-	-	-	-
39/2+	-	-	-	13.61	-	-	-	-

IV. Conclusion

In summary, the structures of $^{185\text{-}187\text{-}189}$Os isotopes have been studied by two important quantities, including nucleon alignments and ratios of reduced transition probabilities, B (E2)/B (M1), up to spins 47/2, 33/2, and 31/2 using the projected shell model, respectively. It was shown in spins 39/2, 33/2, and 29/2, that a pair of protons were aligned by the nucleus equator and an alignment phenomenon occurs occurred. As a result, nucleus rotation frequency decreases and it has a direct effect on directly affects the B(E2)/B(M1) ratio.

By this approach that, in these spins, a slight increase in this ratio is coincident with band

crossing; indeed, electromagnetic transitions occur more due to the electrical property of the nucleus than magnetic.

Besides this, by increasing neutron number, the deformation parameter, ε_2 decrease as well. This means that the rotational state of the isotopes' shape was reduced and take vibration mode slightly. Indeed, ^{189}Os rather than ^{185}Os has had a less spherical-shape, and the rotation alignment happens at lower spins.

Reference

1. R.F. Casten. *Nuclear structure from a simple perspective*. Oxford, New York, (1990).
2. D. Ram, R. Devi, S. K. Khosa, *Microscopic study of positive-parity yrast bands of 224-234Th isotopes*. Pramana. 80, **953** (2013).
3. A. R. Binesh, S. Mohammadi, *Analysis of the Heavy Nuclei Levels with the Newest Data*. Res. J. Phys. 3, **32** (2009).
4. S. Mohammadi, Zs. Podolyak, G. De Angelis, et al., *High-Spin satates populated in Deep-Inelastic Reactions*. Braz. J. Phys. 34, **792** (2004).
5. S. Mohammadi, G. De Angelis, M. Axiotis, et al., *Yrast states in 188,190Os Nuclei*. Int. J. of Mod. Phys. E. 15, **1797** (2006).
6. S. Mohammadi, *High-Spin satates in Deep-Inelastic and Compound-Nucleus Reactions*. Iran. J. Sci. Thec. 34, **13** (2010).
7. S. Mohammadi, Zs. Podolyak, *High spin states in 191Os*. Iran. J. Sci. Thec. 31, **1** (2007).
8. S.G. Nilsson, *Binding States of Individual Nucleons in Strongly Deformed Nuclei Math*. Phys. Medd. 29, **3** (1955).
9. K. Hara, Y. Sun, *Projected Shell Model and High-spin Spectroscopy*. Int. J. Mod. Phys. E 4, **637** (1995).
10. Y. Sun, K. Hara. *Fortran Code of the projected Shell Model: feasible shell model calculation for heavy nuclei. Comput.* Phys. Commun. 104, **245** (1997).
11. M. Shahriarie, S. Mohammadi, Z. Firouzi, *Study of back bending in 157-158 Er isotopes by using Electromagnetic Reduced Transition Probabilities.* J. Korean Phys. Soc. 76, **8** (2020).
12. Moonesi, A. Haghpeima, M. Shahriari, *Study of nucleon-rich effect in 158Er and 185Os rare-earth nuclei using the projected shell model*. J. Korean Phys. Soc. 78, **651** (2021)
13. J. Bardeen, L. N. Cooper, J. R. Schrieffer, *Theory of Superconductivity*. Phys. Rev. 108, **1175** (1957).
14. P. Möller, A.J. Sierk, T. Ichikawa ,et al., *Nuclear ground-state masses and deformations: FRDM(2012*). At. Data Nucl. Data Tables. 109, **1** (2016).
15. J. A. Sheikh, Y. Sun, P. M. Walker, *Projected shell model analysis of tilted rotation*. Phys. Rev. C 75, R**26** (1998).
16. T. Shizuma, S. Mitarai, G. Sletten, et al., *High-spin structure in 185Os.* Phys. Rev. C 69, **024305** (2004).
17. Radware,https://radware.phy.ornl.gov/pub/nd/187/187Os_ensdf_A.ags.
18. Y. Sun, J. Egido. *Angular-Momentum-projected description of the yrast line of dysprosium isotopes*. Nucl. Phys. A 580, **1** (1994).
19. P. Verma, Ch. Sharma, S. Singh, et al., *Projected shell model study of quasiparticle structure of arsenic isotopes*, Nucl. Phys. A 918, **1** (2013).
20. A. Bohr, B. R. Mottelson, *Nuclear Structure*, Vol. I, Sec. 3, World Scientific, Singapore/New Jersey/ London/Hong Kong (1198).
21. B. Castel, I. S. Towner, *Modern Theories of Nuclear Moments.* Sec. 3 and 4, Clarendon, Press Oxford, (1990).
22. B. Alex, *Lecture Notes in Nuclear Structure Physics*, Sec 4, National Superconducting Cyclotron Laboratory and Department of Physics and Astronomy, (2005).

How to cite this article
M. Moonesi, S. Mohammadi, M. Shahriari, Shape Changes in Odd-Even Osmium Isotopes, *Journal of Nuclear Science and Applications,* Vol. **2,** No. **3, (2022),** P **11-18, Url: https://jonra.nstri.ir/article_1414.html, DOI**: 10.24200/jon.2022.1021.